Magnetic and transport properties of a coupled Hubbard bilayer with electron and hole doping

K. Bouadim,[1] G. G. Batrouni,[1] F. Hébert,[1] and R. T. Scalettar[2]
[1]*INLN, Université de Nice-Sophia Antipolis, CNRS, 1361 route des Lucioles, 06560 Valbonne, France*
[2]*Physics Department, University of California, Davis, California 95616, USA*
(Received 11 February 2008; published 30 April 2008)

The single band, two-dimensional Hubbard Hamiltonian has been extensively studied as a model for high temperature superconductivity. While quantum Monte Carlo simulations within the dynamic cluster approximation are now providing considerable evidence for a *d*-wave superconducting state at low temperature, such a transition remains well out of reach of finite lattice simulations because of the "sign problem." We show here that a bilayer Hubbard model, in which one layer is electron doped and one layer is hole doped, can be studied to lower temperatures and exhibits an interesting signal of *d*-wave pairing. The results of our simulations bear resemblance to a recent report on the magnetic and superconducting properties of $Ba_2Ca_3Cu_4O_8F_2$ which contains both electron and hole doped CuO_2 planes. We also explore the phase diagram of bilayer models in which each sheet is at half-filling.

DOI: 10.1103/PhysRevB.77.144527 PACS number(s): 71.10.Fd, 71.30.+h, 02.70.Uu

I. INTRODUCTION

The single band, two-dimensional Hubbard Hamiltonian provides one possible microscopic model for pairing, which is driven by electronic correlations rather than the interactions of electrons with the lattice. Many analytic and numeric[1] treatments suggest that there may indeed be a superconducting phase at low temperature away from half-filling in this model. The issue is a difficult one, however, owing to the likely existence of a variety of different phases which are close in energy on the one hand and the nature of the approximations made in the solution on the other. Exact diagonalization studies,[2,3] while very useful, are typically on lattices of only a few tens of sites, and hence finite size effects are a considerable concern. Quantum Monte Carlo (QMC),[4,5] which can, in principle, address the issue in an unbiased way (on lattices, an order of magnitude or more larger than diagonalization), has been unable to sufficiently access low temperatures due to the "minus sign problem."[6]

Recently, progress has been made by using improved numerical methods. The "density matrix renormalization group" has pushed forward from one dimension to address geometries of many coupled chains.[7] The dynamic cluster approximation has improved on dynamical mean field treatments by showing the robustness of a finite temperature transition to a superconducting state as an increasingly fine momentum grid is incorporated in the self-energy.[8] Nevertheless, there is still numerical work which contests the conclusion that the two-dimensional Hubbard Hamiltonian has long range *d*-wave pair correlations.[9]

In this paper, we present determinant quantum Monte Carlo (DQMC) calculations of a bilayer Hubbard model for which we are able to attain much lower temperatures than the single layer case. Specifically, by symmetrically doping the two layers about half-filling, $\rho=1$, we find that the sign problem is greatly reduced, allowing simulations at temperatures that are roughly 2 orders of magnitude below the bandwidth, $T\approx W/100$. In single layer simulations of the doped system, the lowest attainable temperatures are $T\approx W/40$. Previous DQMC studies of bilayer models have looked at the case when both layers are half-filled and examined the magnetic order-disorder transitions that occur as the interlayer hopping is increased.[10] A decreasing interlayer hopping monotonically reduces the pairing correlations in this situation.

Our work is partially motivated by studies of $Ba_2Ca_3Cu_4O_8F_2$ and $Ba_2Ca_2Cu_4O_6F_2$ which are an experimental realization of materials in which electron and hole doped sheets coexist within the family of cuprate superconductors.[11] In the former, four-layered compound, the two outer planes are electron doped with $N_e\approx 0.06-0.08$, while the two inner planes are hole doped roughly symmetrically, which is $N_h\approx 0.06-0.08$. The superconducting transition temperature is $T_c=55$ K, and pairing coexists with long range antiferromagnetic (AF) order with Néel temperature $T_N=100$ K. The latter, three-layered compound has outer plane doping $N_e\approx 0.06-0.08$ but have larger inner plane doping $N_h\approx 0.13$. Its superconducting $T_c=76$ K, with only short range antiferromagnetic correlations. This is attributed to a decoupling of the magnetism of the electron doped outer planes by the large doping of the inner plane.[11]

II. MODEL AND METHODOLOGY

In order to model such materials, we consider the two layer Hubbard Hamiltonian,

$$H=-t\sum_{\langle \mathbf{i},\mathbf{j}\rangle m\sigma}(c^{\dagger}_{\mathbf{j}m\sigma}c_{\mathbf{i}m\sigma}+\text{H.c.})-t_{\perp}\sum_{\mathbf{i}\sigma}(c^{\dagger}_{\mathbf{i}1\sigma}c_{\mathbf{i}2\sigma}+\text{H.c.})$$
$$-\sum_{\mathbf{i}m\sigma}\mu_m n_{\mathbf{i}m\sigma}+U\sum_{\mathbf{i}m}\left(n_{\mathbf{i}m\uparrow}-\tfrac{1}{2}\right)\left(n_{\mathbf{i}m\downarrow}-\tfrac{1}{2}\right). \quad (1)$$

The first term is the usual hopping of electrons between near neighbor sites $\mathbf{i}$ and $\mathbf{j}$ of a two-dimensional square lattice. The hopping parameter t sets the energy scale: we take $t=1$ in what follows. Unless otherwise stated, the results in this paper are for two coupled 8×8 lattices. The electrons in the kinetic energy term have a spin index $\sigma=\uparrow,\downarrow$ and also a layer index $m=1,2$. The second term is an interlayer hopping. The third term is a layer-dependent chemical potential. We will choose $\mu_1=-\mu_2$ to produce layers that have opposite

dopings. Finally, electrons of opposite spin on the same site of the same layer feel a repulsion U.

Our simulations employ the DQMC algorithm[5,12] in which a path integral is written for the partition function, the fermion interactions are replaced by a coupling to an auxiliary Hubbard–Stratonovich field, and then the fermion degrees of freedom are analytically integrated out. The method produces exact results on the lattice sizes considered, apart from the "Trotter" errors associated with the imaginary time discretization, which we have verified are smaller than our statistical error bars.

The magnetic properties are determined from the spin-spin correlations,

$$c(\mathbf{l}) = \langle M^z_{\mathbf{j}+\mathbf{l},m} M^z_{\mathbf{j},m} \rangle,$$

$$M^z_{\mathbf{j},m} = n_{\mathbf{j}m\uparrow} - n_{\mathbf{j}m\downarrow}, \tag{2}$$

which are independent of layer index m because of our choice of symmetric doping and the particle-hole symmetry of the Hubbard Hamiltonian. The Fourier transform gives the structure factor,

$$S(\mathbf{q}) = \sum_{\mathbf{l}} e^{i\mathbf{q}\cdot\mathbf{l}} c(\mathbf{l}). \tag{3}$$

At half-filling, $S(\mathbf{q})$ is largest at the antiferromagnetic wave vector $\mathbf{q}=(\pi,\pi,\pi)$.

A first insight into the metal-insulator transition can be obtained from the zero momentum spectral function (density of states) $A(\omega)$ which is determined from the Green's function,

$$G_{\mathbf{i}\text{-}\mathbf{j},m\sigma}(\tau) = \langle c_{\mathbf{i}m\sigma}(\tau) c^\dagger_{\mathbf{j}m\sigma}(0) \rangle,$$

$$G_{\mathbf{k}m\sigma}(\tau) = \sum_{\mathbf{l}} e^{i\mathbf{k}\cdot\mathbf{l}} G_{\mathbf{l}m\sigma}(\tau),$$

$$A(\omega) = \int_0^\beta d\tau \frac{e^{-\omega\tau}}{e^{\beta\omega}+1} \sum_{m\sigma} G_{\mathbf{k}=\mathbf{0},m\sigma}(\tau), \tag{4}$$

using the maximum entropy method.[13]

The dc conductivity σ_{dc} also characterizes the metal-insulator transition and is measured from the current-current correlation function,

$$j_x(\mathbf{l},\tau) = e^{H\tau} j_x(\mathbf{l},0) e^{-H\tau},$$

$$j_x(\mathbf{l},0) = it \sum_{m\sigma} (c^\dagger_{\mathbf{l}+x m\sigma} c_{\mathbf{l}m\sigma} - c^\dagger_{\mathbf{l}m\sigma} c_{\mathbf{l}+x m\sigma}),$$

$$\Lambda_{xx}(\mathbf{q};\tau) = \sum_{\mathbf{l}} e^{i\mathbf{q}\cdot\mathbf{l}} \langle j_x(\mathbf{l},\tau) j_x(0,0) \rangle. \tag{5}$$

This imaginary time quantity, which directly comes out of the determinant QMC simulations, is related to the real frequency response by the fluctuation-dissipation theorem,

$$\Lambda_{xx}(\mathbf{q};\tau) = \int_{-\infty}^{+\infty} \frac{d\omega}{\pi} \frac{e^{-\omega\tau}}{1-e^{-\beta\omega}} \mathrm{Im}\, \Lambda_{xx}(\mathbf{q},\omega). \tag{6}$$

As discussed in Ref. 14, at sufficiently low temperatures, we can replace $\mathrm{Im}\,\Lambda$ by its low frequency behavior $\mathrm{Im}\,\Lambda \approx \sigma_{\mathrm{dc}}\omega$, leading to the relation,

$$\Lambda_{xx}\left(\mathbf{q}=0;\tau=\frac{\beta}{2}\right) = \frac{\pi\sigma_{\mathrm{dc}}}{\beta^2}. \tag{7}$$

This enables us to directly obtain the conductivity from the imaginary time response without the necessity for analytic continuation, which is more difficult for two particle response functions, such as the current-current correlator, than for the single particle Green's function, owing to their larger fluctuations.

To describe superconductivity, we compute the correlated pair field susceptibility P_α in different symmetry channels,

$$P_\alpha = \int_0^\beta d\tau \langle \Delta_\alpha(\tau) \Delta^\dagger_\alpha(0) \rangle,$$

$$\Delta^\dagger_\alpha = \frac{1}{N} \sum_{\mathbf{k}} f_\alpha(\mathbf{k}) c^\dagger_{\mathbf{k}\uparrow} c^\dagger_{-\mathbf{k}\downarrow},$$

$$f_s(\mathbf{k}) = 1,$$

$$f_{s*}(\mathbf{k}) = \cos k_x + \cos k_y,$$

$$f_d(\mathbf{k}) = \cos k_x - \cos k_y. \tag{8}$$

The correlated susceptibility P_α takes the expectation value of the product of the four fermion operators entering Eq. (8). We also define the uncorrelated pair field susceptibility $\bar{P}_\alpha$ that instead computes the expectation values of pairs of operators prior to taking the product. Thus, for example, in the s-wave channel,

$$P_s = \frac{1}{N^2} \sum_{\mathbf{i},\mathbf{j}} \int_0^\beta d\tau \langle c_{\mathbf{i}\downarrow}(\tau) c_{\mathbf{i}\uparrow}(\tau) c^\dagger_{\mathbf{j}\uparrow}(0) c^\dagger_{\mathbf{j}\downarrow}(0) \rangle,$$

$$\bar{P}_s = \frac{1}{N^2} \sum_{\mathbf{i},\mathbf{j}} \int_0^\beta d\tau \langle c_{\mathbf{i}\downarrow}(\tau) c^\dagger_{\mathbf{j}\downarrow}(0) \rangle \langle c_{\mathbf{i}\uparrow}(\tau) c^\dagger_{\mathbf{j}\uparrow}(0) \rangle. \tag{9}$$

Here, P_α includes both the renormalization of the propagation of the individual fermions as well as the interaction vertex between them, whereas $\bar{P}_\alpha$ includes only the former effect. Indeed, by evaluating both P and $\bar{P}$, we are able to extract[15] the interaction vertex Γ,

$$\Gamma_\alpha = \frac{1}{P_\alpha} - \frac{1}{\bar{P}_\alpha}. \tag{10}$$

If $\Gamma_\alpha \bar{P}_\alpha < 0$, the associated pairing interaction is attractive. In fact, rewriting Eq. (10) as

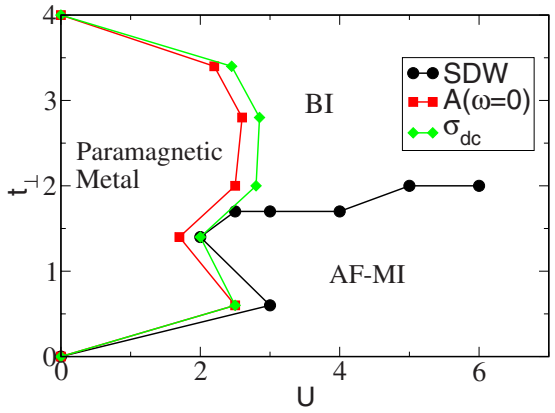

FIG. 1. (Color online) Phase diagram for the half-filled bilayer Hubbard model. A paramagnetic metallic phase is present at weak coupling. At large coupling, there is a transition from an antiferromagnetic Mott-insulating phase to a paramagnetic band-insulating phase. The phase boundaries obtained by the conductivity σ and density of states at the Fermi level, $A(0)$, are consistent.

$$P_\alpha = \frac{\bar{P}_\alpha}{1 + \Gamma_\alpha \bar{P}_\alpha} \tag{11}$$

suggests that $\Gamma_\alpha \bar{P}_\alpha \to -1$ signals a superconducting instability. We will discuss this criterion in more detail in Secs. IV and V.

III. BILAYER PHASE DIAGRAM AT HALF-FILLING

We begin with the phase diagram at half-filling, which is when $\mu_1 = \mu_2 = 0$ and both layers have equal occupation $\rho_1 = \rho_2 = 1$. (Note that there is no sign problem in this case because of particle-hole symmetry.) Here, we do not expect superconductivity. Nevertheless, there is an interesting competition between Mott insulating behavior when U is the dominant energy scale and band insulating behavior for large $t_\perp$. Indeed, increased interlayer coupling suppresses the antiferromagnetic correlations that are present in the Mott phase, since $t_\perp$ promotes the formation of interlayer singlets between the two spatial sites immediately above and below each other. These spin-0 singlets are magnetically decoupled, destroying long range spin order. Earlier determinant QMC studies determined the critical value of $t_\perp \approx 1.6$ for this AF-paramagnetic transition.[10]

The strong coupling region of Fig. 1 exhibits this phenomena and yields a $t_{\perp c}$ consistent with the earlier study.[10] At weak coupling, however, this insulator-insulator transition is replaced by a metallic phase. Previous cluster dynamical mean field theory (DMFT)[16] studies of the bilayer model show a phase diagram that is in qualitative agreement with Fig. 1. We will compare the results of the two methods in more detail at the end of Sec. III. First, we will describe in detail how this phase diagram is obtained.

In Fig. 2, the density of states at the Fermi surface, $A(\omega = 0)$, is shown for four temperatures along a horizontal cut through the phase diagram at fixed $t_\perp = 2$. At weak coupling, the low temperature limit is nonzero, which indicates a metallic phase, while at strong coupling, $A(\omega = 0)$ decreases as T is lowered. We conclude that at the crossing point $U \approx 2.8$, a metal-insulator transition occurs.

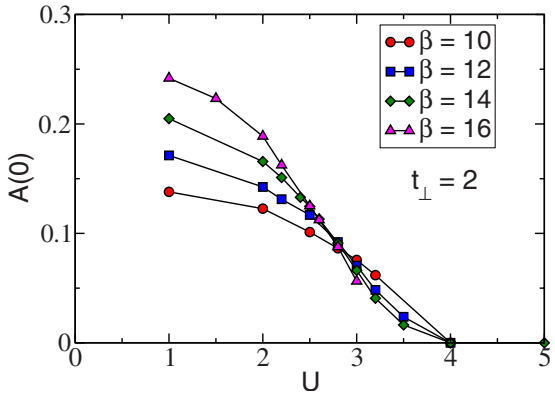

FIG. 2. (Color online) Density of states at the Fermi surface $A(0)$ for $t_\perp = 2$. At weak U, $A(0)$ rises as $T = 1/\beta$ is lowered, indicating a metallic phase with nonzero Fermi level density of states. In contrast, at large U, $A(0)$ falls with decreasing T, indicating insulating behavior. $U_c \approx 2.8$.

In Fig. 3, we see that the conductivity σ_{dc} similarly can determine the location of the metal-insulator phase boundary. Here, a change in the temperature behavior of the conductivity, from increasing as T is lowered (metallic) to decreasing when T is lowered (insulating), occurs at $U \approx 2.6$ when the interlayer hopping is $t_\perp = 3.4$.

Multiple horizontal (constant $t_\perp$) cuts through the phase diagram similar to those of Figs. 2 and 3 were used to generate the metal-insulator phase boundary of Fig. 1. Note the consistency of the locations of the critical interaction strengths between those obtained from the density of states $A(\omega = 0)$ (red squares in Fig. 1) and the conductivity σ_{dc} (green diamonds in Fig. 1).

In this bilayer model, at half-filling $\mu_1 = \mu_2 = 0$, the suppression of the zero frequency spectral weight can come

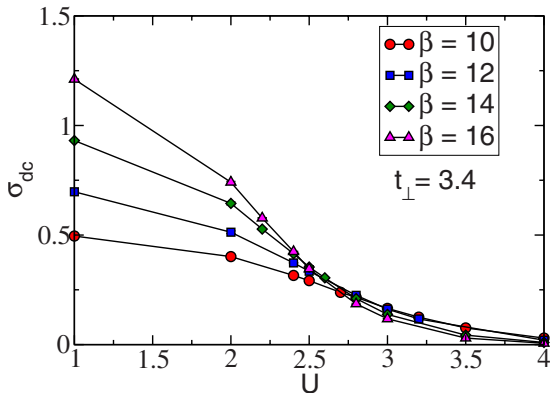

FIG. 3. (Color online) The conductivity σ_{dc} for a horizontal cut (fixed $t_\perp = 3.4$) and varying U through the phase diagram. Values at four inverse temperatures are given. As with the density of states at the Fermi energy, $A(\omega = 0)$, as shown in Fig. 2, the conductivity exhibits a crossing pattern that gives the location of the metal-insulator phase boundary: σ_{dc} increases as β increases (metallic behavior) below $U \approx 2.6$ and falls as β increases above this value.

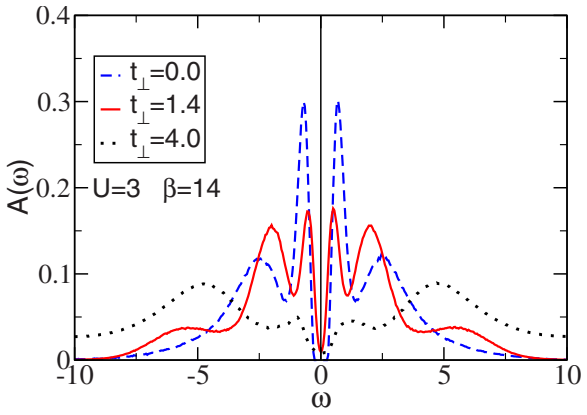

FIG. 4. (Color online) Density of states $A(\omega)$ at $U=3$ and inverse temperature $\beta=14$, showing insulating behavior at all values of interlayer coupling. $t_\perp=0$ and $t_\perp=1.4$ are Mott/Slater insulating phases with a gap produced by a combination of the on-site repulsion and antiferromagnetic spin correlations. $t_\perp=4.0$ has a gap which is primarily band insulator in character.

from any of three mechanisms: the opening of a band gap at sufficiently large $t_\perp$, a "Slater gap" created by antiferromagnetic fluctuations which can form on a scale set by the exchange constant $J \propto t^2/U$, and a "Mott gap" between the upper and lower Hubbard bands when U exceeds the bandwidth W. (The bandwidth $W=8t$ at $t_\perp=0$.) In general, these different insulating phases cross over to each other more or less smoothly, although the Slater insulator can be distinguished by the presence of long range spin correlations. Figure 4 shows the full frequency dependence of the density of states at $U=3$ and three values of $t_\perp$, all of which exhibit a gap in $A(\omega)$. [The nonzero residual values of $A(\omega)$ for $t_\perp=1.4$ and 4.0 will be driven to zero if β is increased; see Fig. 2.] From Fig. 4, we infer that the phase diagram is insulating all along the vertical line $U=3$ in Fig. 1.

In contrast, Fig. 5, which shows the same three values of $t_\perp$ except at weaker coupling, $U=2$, clearly exhibits metallic behavior for the intermediate value of the interlayer hopping. This is one indication of the outward extent of the metallic region from $U=0$ in the phase diagram of Fig. 1.

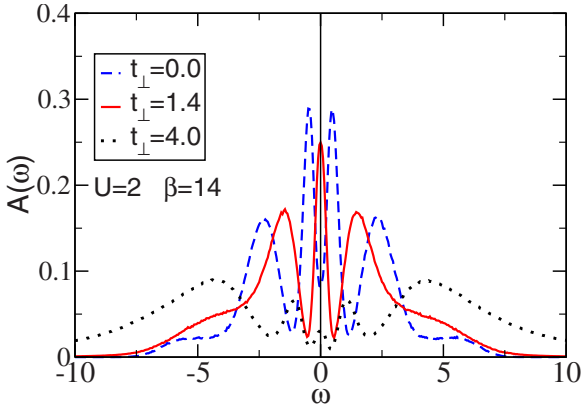

FIG. 5. (Color online) The same as Fig. 4, except $U=2$. Although $t_\perp=0.0$ and 4.0 are still insulating, the density of states for $t_\perp=1.4$ has a peak at $\omega=0$ and is metallic in character.

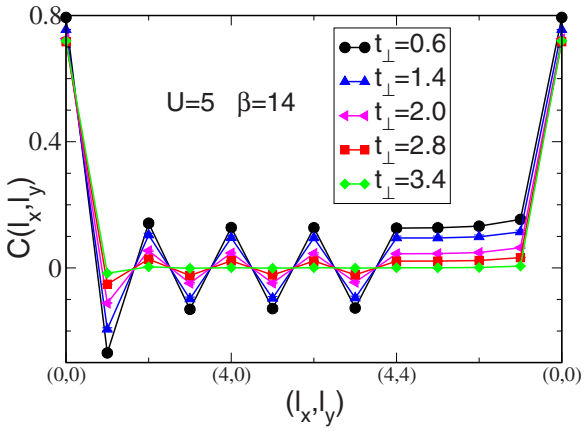

FIG. 6. (Color online) Real space spin correlations at $U=5$. As $t_\perp$ increases, the antiferromagnetism is suppressed. The inverse temperature $\beta=14$.

We turn now to the spin correlations. Figure 6 shows the real space spin correlations for $U=5$ and different interlayer hoppings. $t_\perp$ drives the formation of interlayer singlets which interfere with the magnetic order. A finite size scaling analysis is shown in Fig. 7 where the structure factor is plotted as a function of the inverse linear system size. Spin wave theory predicts[17] that the finite size corrections to $S(\pi,\pi,\pi)$ should be linear in $1/N_x$, with the $N_x \to \infty$ intercept proportional to the square of the order parameter. We see that the order parameter is nonzero for $t_\perp=0.6$ and 1.4 and is zero for $t_\perp=2.8$ and 3.4. Somewhere in the vicinity of $t_\perp \approx 2$, the long range magnetic order is destroyed. Figure 8 shows a similar finite size scaling analysis for weaker coupling, $U=2$. There is no long range magnetic order for any value of $t_\perp$.

The finite size scaling analysis in these figures is identical to that used by Hirsch and Tang[18] in their seminal study which numerically established the existence of long range antiferromagnetic order in the ground state of the half-filled single band Hubbard model.

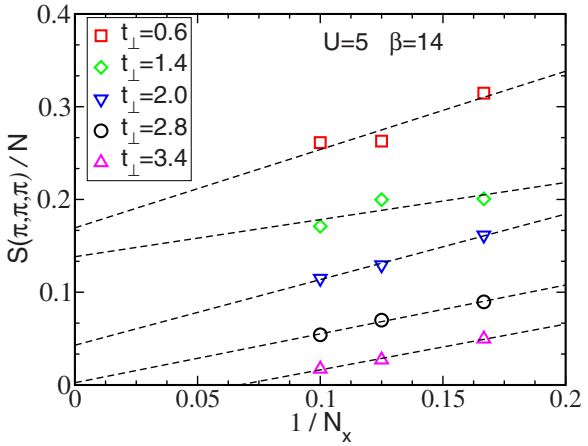

FIG. 7. (Color online) Scaling of the antiferromagnetic structure factor at $U=5$. If there are long range correlations, $S(\pi,\pi,\pi)$ should linearly grow with lattice size N, so that $S(\pi,\pi,\pi)/N$ approaches a constant for large N. Spin wave theory predicts a $1/N_x$ correction, where N_x is the linear lattice size ($N_x^2=N$). Here, we see long range order for the three smallest values $t_\perp=0.6$, 1.4, and 2.0, but not for the two largest values $t_\perp=2.8$, and 3.4.

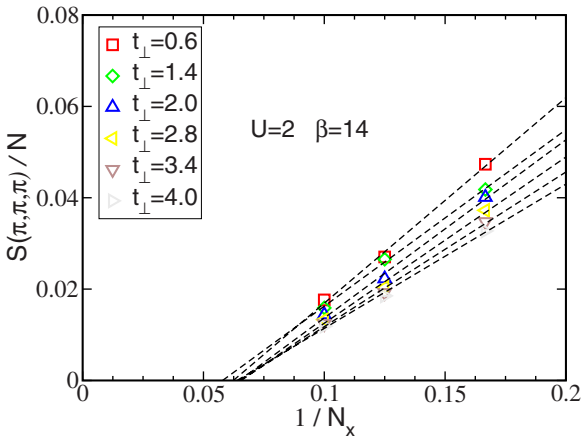

FIG. 8. (Color online) Same as Fig. 7 except $U=2$.

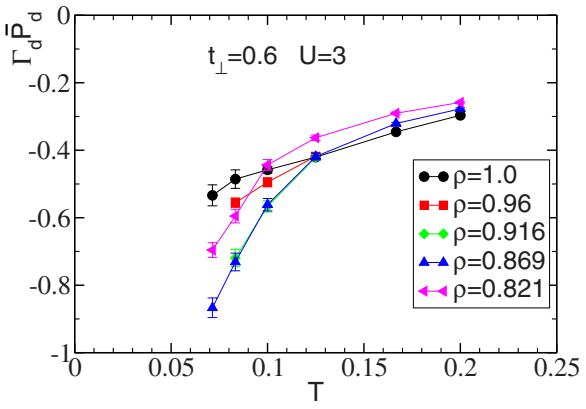

FIG. 9. (Color online) d-wave pairing vertex as a function of temperature for two 8×8 bilayers with interlayer hopping $t_\perp=0.6$. The on-site interaction $U=3$. Three fillings are shown. Note the close approach to $\Gamma\bar{P}=-1$, the onset point of a pairing instability, and the nonmonotonic dependence on filling. The greatest tendency to pairing is at $\rho\approx0.87$.

Multiple vertical (constant U) cuts through the phase diagram similar to those of Figs. 6–8 were used to generate the limit of the antiferromagnetically ordered regions of the phase diagram (Fig. 1). This value is consistent with previous DQMC studies[10] and cluster DMFT.[16]

We conclude Sec. III with a more quantitative comparison of Fig. 1 with the results obtained in cluster DMFT.[16] At strong coupling, the AF insulator to paramagnetic (bond) insulator transition is found by both methods to have the same value $t_\perp=2$. Likewise, in both approaches, the base of the metallic phase at $U=0$ extends from $t_\perp=0$ to $t_\perp=4$, as indeed it must analytically from the noninteracting dispersion that has bonding and antibonding bands,

$$\epsilon_1(\mathbf{k}) = -t_\perp + 2t(\cos k_x + \cos k_y),$$

$$\epsilon_2(\mathbf{k}) = +t_\perp + 2t(\cos k_x + \cos k_y). \tag{12}$$

The extent of the metallic phase as U increases from the noninteracting limit quantitatively differs in the two methods. The DQMC results reported here indicate an upper limit of $U\approx3$, while within cluster DMFT, the metallic region extends out to $U\approx8$. The precise origin of this disagreement is not clear. The peak of the cluster DMFT metallic lobe follows the emerging AF-band insulator line rather narrowly, and it is possible that DQMC cannot resolve this small region adequately. While the results of Figs. 2 and 4 seem unambiguously to rule out metallic behavior much beyond $U\approx3$, they are on lattices of finite extent ($N=8\times8$). Cluster DMFT works in the thermodynamic limit and hence typically produces sharper transitions that can distinguish narrow regions of phase space. On the other hand, DQMC incorporates the full momentum dependence of the self-energy, in contrast to the 2×2 momentum grid used in cluster DMFT.

IV. SUPERCONDUCTIVITY IN THE DOPED SYSTEM

Figure 9 shows a central result of our paper. The product of the d-wave pairing vertex and the uncorrelated susceptibility, $\Gamma_d\bar{P}_d$, is seen to turn sharply negative (attractive) as the temperature T is lowered. As described in Eq. (11), $\Gamma_d\bar{P}_d\rightarrow-1$, in principle, would signal a superconducting instability. For $\rho\approx0.87$, $\Gamma_d\bar{P}_d\approx-0.9$. In comparison, the most negative $\Gamma_d\bar{P}_d$ reported[15] for the single band model is $\Gamma_d\bar{P}_d=-0.45$ at half-filling, $\rho=1.000$, and $\Gamma_d\bar{P}_d=-0.25$ for doping to $\rho=0.875$. It should be kept in mind, however, that the lowest accessible temperature in the latter case is $\beta=6$. At the same $\beta=6$ and doping $\rho=0.875$, as seen in Fig. 9, the bilayer system has a somewhat more negative $\Gamma_d\bar{P}_d=-0.31$. Thus, the approach of $\Gamma_d\bar{P}_d$ to -1 seen in the bilayer system is not only due both to a more attractive pairing vertex but also due to the ability of the simulation to reach much colder temperatures.

Although we find the vertex $\Gamma_d\bar{P}_d$ approaches -1, this criterion for an instability is incomplete. One also needs to require that the uncorrelated susceptibility $\bar{P}$ remains finite at the transition point. Especially in the situation where there is competing order (e.g., antiferromagnetism and pairing), it is possible for the uncorrelated susceptibility of one type of order to be driven to small values by the other order, so that even though the vertex approaches -1, order in this channel is usurped. Figure 10 addresses this issue for the bilayer model. Despite the fact that $\Gamma_d\bar{P}_d$ is getting close to -1, the correlated vertex P_d grows relatively slowly as T is decreased. The reason is clear from Fig. 10 in which it is seen that the uncorrelated susceptibility is rapidly dropping as T is lowered. This is rather different from the doped single layer model, where $\bar{P}_d$ grows as T is lowered. (At half-filling in the single layer model, $\bar{P}_d$ slightly declines as T is decreased, as found here also in the bilayer model.)

An interesting feature of Figs. 9 and 10 is that the d-wave attraction is maximal at $\rho\approx0.87$, whether measured via the vertex or the correlated susceptibility. This point is more concretely made in Fig. 11. The behavior of the d-wave superconducting vertex bears an interesting resemblance to the superconducting "domes" of the cuprate materials in which the transition temperatures are maximized in a finite distance away from "half-filling" (one hole per Cu). Indeed, even the

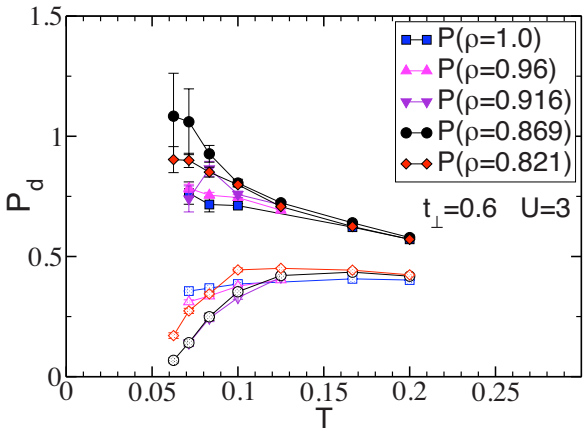

FIG. 10. (Color online) Correlated (closed symbols) and uncorrelated (open symbols) d-wave pairing susceptibility as a function of temperature for two 8×8 bilayers with interlayer hopping $t_\perp=0.6$. The on-site interaction $U=3$. Five fillings are shown. In all cases, the vertex is attractive, i.e., $P_d > \bar{P}_d$. The degree of attraction is nonmonotonic, first increasing with doping, but then declining.

values of the doping which maximize T_c and the width of the base of the dome are in reasonable quantitative agreement. It is to be emphasized that, within the same DQMC methodology, the single layer Hubbard model has a maximum pairing vertex at half-filling. Figure 11 also indicates that, within the parameter range accessible, the degree of enhancement increases as $t_\perp$ decreases. Eventually, we expect this trend to reverse, since at $t_\perp=0$, the single layer model, there is a lesser tendency for pairing. (We cannot accumulate data for smaller values of $t_\perp$ because the sign problem prevents simulations at as low a temperature as for the data shown.)

We turn now to the magnetic properties of the doped system and, in particular, their connection to those observed in the cuprate superconductors. Figure 12 shows the real space spin-spin correlations for $\rho=1.00$, 0.96, 0.92, 0.87, and 0.82 at $\beta=8$, $U=3$, and $t_\perp=0.6$. These results have a quantitative similarity to the $Ba_2Ca_3Cu_4O_8F_2$ and $Ba_2Ca_2Cu_4O_6F_2$ materials in that the robust magnetic correlations present for ρ

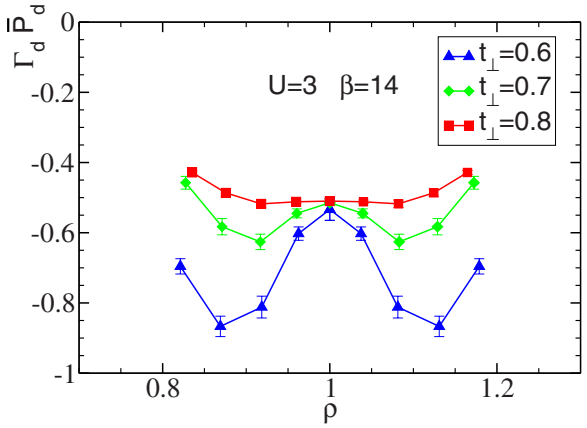

FIG. 11. (Color online) d-wave pairing vertex as a function of filling for two 8×8 bilayers with interlayer hopping $t_\perp=0.6$, 0.7, and 0.8. The on-site interaction $U=3$ and inverse temperature $\beta=14$. The greatest tendency to pairing is at $\rho\approx0.87$.

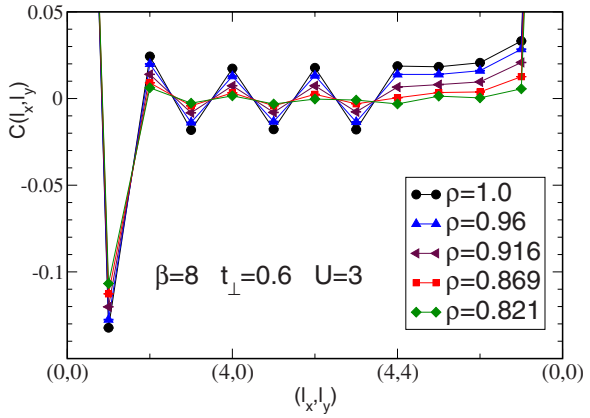

FIG. 12. (Color online) Real space spin correlations. At half filling, $\rho=1.00$, and for small dopings, $\rho=0.96$, there is a strong oscillatory pattern that is indicative of long range magnetic order (Ref. 19). For larger dopings, the spin correlations are sharply curtailed.

$=1.00$ and $\rho=0.96$ are dramatically suppressed for $\rho=0.87$. A finite Neel temperature T_N is present for the four layer compound $Ba_2Ca_2Cu_4O_6F_2$ which has electron and hole dopings N_e, $N_h\approx0.06$ and absent for the three layer compound $Ba_2Ca_2Cu_4O_6F_2$ which has hole doping $N_h\approx0.14$ in the central layer.

Why is the sign problem ameliorated in these bilayer simulations? In DQMC for the single layer Hamiltonian, the operator $n_{i\uparrow}$ couples to the Hubbard–Stratonovich field h_i (Ref. 20) shifted by the chemical potential $h_i-\mu$. Meanwhile, $n_{i\downarrow}$ couples to $-h_i-\mu$. At half-filling, $\mu=0$, particle-hole symmetry is reflected in the fact that the up and down species couple to the quantities $\pm h_i$ which are symmetric about zero. The up and down determinants can be shown to have the same sign, and hence their product is positive. For $\mu\neq0$, this symmetry and the associated connection between the signs of the two determinants are broken, and a sign problem results. (Note that for the attractive Hubbard Hamiltonian, $n_{i\uparrow}$ and $n_{i\downarrow}$ both couple to $h_i-\mu$ and the two determinants are equal at all fillings.)

Consider now the bilayer system. We have a Hubbard–Stratonovich field for each layer. The operators $n_{i1\uparrow}$ couple to $h_{i1}-\mu$, while $n_{i1\downarrow}$ couple to $-h_{i1}-\mu$ and $n_{i2\uparrow}$ couple to $h_{i2}+\mu$, and finally $n_{i2\downarrow}$ couple to $-h_{i2}+\mu$, where we have explicitly set $\mu_1=-\mu_2=-\mu$. What we observe is that to the extent that the Hubbard–Stratonovich variables on the two layers are equal, $n_{i1\uparrow}$ and $n_{i2\downarrow}$ are symmetrically coupled about zero. It is possible that this tends to lead to a positive determinant product similar to the single layer case at half-filling. Of course, there is no constraint that $h_{i1}=h_{i2}$, but we suspect that they are nevertheless sufficiently correlated to reduce the sign problem.

V. CONCLUSIONS

In this paper, we have used DQMC simulations to determine the phase diagram, in the $(t_\perp, U)$ plane, of the half-filled bilayer Hubbard model. Our phase diagram exhibits metallic, band insulating and Mott insulating phases in quali-

tative agreement with CDMFT results.[16] However, the entire metallic phase we find is paramagnetic with no antiferromagnetic metallic regions.

In addition, we have shown that the doped bilayer Hubbard Hamiltonian has an attractive d-wave pairing vertex that approaches close to $\Gamma_d \bar{P}_d = -1$, signaling a superconducting transition. This value is much more singular than that observed in the single layer model partly because it is more attractive when compared to the same inverse temperature and partly because it is possible to simulate to values of β which are two to three times larger than for a single plane. However, the uncorrelated $\bar{P}_d$ gets small, so that the enhancement of the correlated P_d is not very dramatic. On the other hand, and unlike what happens in the single layer $d=2$ Hubbard model, the enhancement here is maximum when the system is doped, in agreement with the phenomenology of cuprate superconductors.

Pairing in systems with separate electron and hole doped sheets has a long history in the context of exciton condensation,[21] but our primary motivation here has been the recent report of cuprate-based systems $Ba_2Ca_3Cu_4O_8F_2$ and $Ba_2Ca_2Cu_4O_6F_2$ which have both types of dopings.[11] Our results for the magnetic and pairing correlations bear interesting connections to those materials. While the bilayer simulations reported here contain the essential feature of coupled electron and hole doped layers, it is natural to consider direct numerics of three and four layer compounds. Such studies will require an order of magnitude greater simulation time and also have an at present unknown sign problem. In general, the sign problem becomes worse with lattice size (and hence with number of layers), but as we have shown here, the correlated determinant signs in the layers help keep the average sign larger than for a single doped layer.

ACKNOWLEDGMENTS

K.B., F.H., and G.G.B. acknowledge financial support from a grant from the CNRS (France) (PICS 18796) and R.T.S. from DOE DE-FC0206ER25793. We acknowledge very useful help from M. Schram and K. Dawson. This research was supported in part by the National Science Foundation under Grant No. NSF PHY05-51164.

[1] D. J. Scalapino, in *Handbook of High Temperature Superconductivity*, edited by J. R. Schrieffer (Springer, Berlin, 2006), Chap. 13.
[2] H. Q. Lin, J. E. Hirsch, and D. J. Scalapino, Phys. Rev. B **37**, 7359 (1988).
[3] A. Parola, S. Sorella, S. Baroni, R. Car, M. Parrinello, and E. Tosatti, Physica C **162**, 771 (1989).
[4] J. E. Hirsch and H. Q. Lin, Phys. Rev. B **37**, 5070 (1988).
[5] S. R. White, D. J. Scalapino, R. L. Sugar, E. Y. Loh, J. E. Gubernatis, and R. T. Scalettar, Phys. Rev. B **40**, 506 (1989).
[6] E. Y. Loh, J. E. Gubernatis, R. T. Scalettar, S. R. White, D. J. Scalapino, and R. L. Sugar, Phys. Rev. B **41**, 9301 (1990).
[7] S. R. White and D. J. Scalapino, Phys. Rev. Lett. **80**, 1272 (1998).
[8] M. Jarrell, Th. Maier, C. Huscroft, and S. Moukouri, Phys. Rev. B **64**, 195130 (2001).
[9] T. Aimi and M. Imada, J. Phys. Soc. Jpn. **76**, 113708 (2007).
[10] R. T. Scalettar, J. W. Cannon, D. J. Scalapino, and R. L. Sugar, Phys. Rev. B **50**, 13419 (1994); R. T. Scalettar, J. Low Temp. Phys. **99**, 499 (1995).
[11] S. Shimizu, H. Mukuda, Y. Kitaoka, A. Iyo, Y. Tanaka, Y. Kodama, K. Tokiwa, and T. Watanabe, Phys. Rev. Lett. **98**, 257002 (2007).
[12] R. Blankenbecler, D. J. Scalapino, and R. L. Sugar, Phys. Rev. D **24**, 2278 (1981).
[13] R. N. Silver, D. S. Sivia, and J. E. Gubernatis, Phys. Rev. B **41**, 2380 (1990).
[14] N. Trivedi, R. T. Scalettar, and M. Randeria, Phys. Rev. B **54**, R3756 (1996).
[15] S. R. White, D. J. Scalapino, R. L. Sugar, N. E. Bickers, and R. T. Scalettar, Phys. Rev. B **39**, 839 (1989).
[16] S. S. Kancharla and S. Okamoto, Phys. Rev. B **75**, 193103 (2007).
[17] D. A. Huse, Phys. Rev. B **37**, 2380 (1988).
[18] J. E. Hirsch and S. Tang, Phys. Rev. Lett. **62**, 591 (1989).
[19] Actually, it is likely the model exhibits long range order only at $\rho=1$. Nevertheless, the correlations at $\rho=0.96$ decay very little with increasing separation. In a real material, even weak three dimensional coupling is likely to stabilize the magnetism.
[20] Actually, the Hubbard–Stratonovich field also depends on imaginary time τ, which is a dependence we suppress in this paper.
[21] For two recent articles, see A. V. Balatsky, Y. N. Joglekar, and P. B. Littlewood, Phys. Rev. Lett. **93**, 266801 (2004); K. P. Walsh, A. T. Fiory, N. M. Ravindra, D. R. Harschman, and J. D. Dow, Philos. Mag. **86**, 3581 (2006), and references cited therein.